RESEARCH ARTICLE | JULY 21 2026

The Cahn–Hilliard residuum and its implications for critical-point wetting at solid solution surfaces

Marine Bossert ; Yong Li ; Jörg Weissmüller

J. Chem. Phys. 165, 034706 (2026)
https://doi.org/10.1063/5.0340000

The Journal of Chemical Physics ARTICLE pubs.aip.org/aip/jcp

The Cahn–Hilliard residuum and its implications for critical-point wetting at solid solution surfaces

Cite as: J. Chem. Phys. 165, 034706 (2026); doi: 10.1063/5.0340000
Submitted: 22 April 2026 • Accepted: 1 July 2026 •
Published Online: 21 July 2026

Marine Bossert,[1] Yong Li,[2] and Jörg Weissmüller[1,2,a)]

AFFILIATIONS

[1] Institute of Materials Physics and Technology, Hamburg University of Technology, Hamburg, Germany
[2] Institute of Hydrogen Technology, Helmholtz-Zentrum Hereon, Geesthacht, Germany

[a)] Author to whom correspondence should be addressed: weissmueller@tuhh.de

ABSTRACT

As part of their seminal 1958 analysis of nonuniform solutions, Cahn and Hilliard [J. Chem. Phys. **28**, 258–267 (1958)] identified the Laplacian of the composition field as the key contribution to the excess free energy in solids with a conserved network of discrete atomic sites. Integration by parts converted to the now familiar gradient-square form underlying phase-field simulations and studies of critical-point wetting. The residuum from the integration by parts has since been ignored. Here, we examine its implications using critical-point wetting at the surface of an Ising-type solid solution for a representative case. As a benchmark, atomistic Monte Carlo simulation shows a continuous increase in wetting-layer thickness up to the bulk critical temperature. In contrast, the classical gradient-square continuum model predicts a first-order wetting transition. A more realistic Laplacian-based continuum formulation does not readily admit physically meaningful minimization by standard variational methods. As a discrete approach, a plane-by-plane model with an excess energy based on a second-difference (curvature) operator yields solutions consistent with the benchmark. Summation by parts transforms this operator into a first-difference- (gradient-) square form, and neglect of the residual term again leads to an incorrect first-order transition. Thus, the choice between curvature and gradient-square formulations alters the predicted character—first-order transition or continuous evolution in layer thickness—of the wetting, underscoring the fundamental importance of this choice.

I. INTRODUCTION AND MOTIVATION

In the search for equilibrium configurations of solutions of two elements, it is often favorable to work with a continuum description of the free energy which approximates the energetics of discrete atomic matter. A seminal work by Cahn and Hilliard[1] established gradient energy terms as a quintessential element in continuum approaches to alloy thermodynamics. Gradient energy is relevant to a wide range of problems in condensed matter science, and it forms the basis for phase-field approaches to equilibration and microstructure evolution.[2–4]

Continuum models approximate the true free-energy value, $\tilde{\mathcal{F}}$, of matter with a discrete atomic structure, by a quantity $\mathcal{F}$ derived from integrals of energy density functions Ψ (per volume) and ψ (per area) over the volume, V, and over the surface, S. A fundamental task is to identify the functions or functionals Ψ and ψ that let $\tilde{\mathcal{F}} \equiv \mathcal{F}$. By analyzing the free energy functional in terms of a series expansion, Cahn and Hilliard[1] found that the leading composition-gradient terms in Ψ are proportional to the gradient square and to the second derivative of the solute fraction, x, that is $\Psi = \Psi_0(x) + \kappa_1(x)\Delta x + \kappa_2(x)\,(\nabla x)^2$. They pointed out that this can be simplified to a gradient-square description, since integration by parts transforms[1]

$$\mathcal{F} = \int_V \left(\Psi_0 + \kappa_1\,\Delta x + \kappa_2\,(\nabla x)^2\right) \mathrm{d}v + \int_S \psi\,\mathrm{d}a, \tag{1}$$

to

$$\mathcal{F} = \int_V \left(\Psi_0 + \kappa\,(\nabla x)^2\right) \mathrm{d}v + \int_S \left(\psi + \kappa_1\,(\nabla x)\cdot\mathbf{n}\right) \mathrm{d}a, \tag{2}$$

with $\kappa = \kappa_2 - \mathrm{d}\kappa_1/\mathrm{d}x$ and $\mathbf{n}$ the outer surface normal.

Cahn and Hilliard also inspected the atomic-scale origin of the gradient energy, analyzing a network solid with a conserved array

of sites and with the energy in near-neighbor bonds. When the sites were embedded in a nonuniform composition field, they found bond-counting to imply an excess energy that scales with the second derivative and not with the gradient or its square.[1] This observation implies $\kappa_2 = 0$, and it identifies $\kappa_1(x)$ or (after partial integration) $\kappa = -\mathrm{d}\kappa_1/\mathrm{d}x$ as the pertinent coefficients.

Equation (2), with the gradient-square free energy in the bulk, has been the basis of the vast majority of work building on Ref. 1. The surface residuum term $\kappa_1(\nabla x) \cdot \mathbf{n}$, which is part of this picture, has been consistently ignored. As pointed out in Ref. 1, the residuum is indeed without consequence for composition profiles within the bulk. Yet phenomena at surfaces or interfaces may be affected, and this is the subject of the present work.

A prototypical application of gradient thermodynamics to surfaces is critical-point wetting in solutions with a miscibility gap. Another seminal paper by Cahn[5] concludes that any two-phase system in contact with a third phase will—below its bulk consolute critical temperature, T_C—undergo a wetting transition, where one of the two phases of the system completely wets the third phase. This notion—which may be transferred to related scenarios such as pre-melting or disorder wetting at surfaces or grain boundaries—has been confirmed by many follow-up theory studies.[6–10]

Critical-point wetting was originally suggested as a first-order transition,[5] and this is supported by phase-field simulation that rests upon the Cahn–Hilliard theory.[11–14] Fluid solutions provide ample experimental evidence for the first-order character,[7,8,10,15] including specifically direct observation of the discontinuity in the wetting-layer thickness[16,17] as well as metastability or hysteresis.[18–20] Wetting layers and wetting transitions have also been predicted and observed in solid solutions.[8] Nb–H provides an early experimental example of a solid-state wetting layer.[21] Disorder wetting at anti-phase boundaries in superlattices, such as Cu_3Au, Pt_3Co, and Cu_3Pd, exemplifies first-order wetting transitions.[22]

Closer inspection reveals that the character of the wetting transition depends sensibly on the nature of the interactions. In addition to discontinuous (first-order) transitions, theory points to gradual (second order[7] or "critical"[6,9,10]) transitions. This latter scenario has been observed in experiment with organic fluid mixtures.[17,23,24] While the wetting temperature is typically predicted distinctly below the bulk T_C, Ising[25] as well as phase-field[13,26] models can suggest a continuous increase of the wetting layer thickness with divergence only at T_C ("continuous wetting"[27]). This was observed for disorder wetting at the outer surface of Cu_3Au.[28,29] The suppression ("nonwetting gap" in a finite interval of the wall-fluid interaction strength) of a wetting transition proper, in favor of continuous wetting, has also been argued to result when short- and long-range forces act simultaneously within the bulk and at the surface, respectively.[27,30,31]

Wetting at planar solid interfaces can be studied in (crystal-lattice) plane-by-plane models with 1D gradients and mean-field expressions for the free energy of each plane.[25,32–37] Such models often suggest a series of layering transitions.[25,32–35]

Numerical approaches to atomic-scale models for wetting in solids include on-lattice[38–43] and off-lattice[44] Monte Carlo simulations. Some studies support the continuous thickening of the wetting layer and the divergence at the bulk T_C,[39,40] while others demonstrate a pre-wetting line and, hence, a first-order wetting transition below T_C.[42] A dedicated comparison finds qualitative differences between the predictions of Monte Carlo and phase-field approaches for nominally the same scenario.[44]

Wetting-related transitions in solids are sensitive to the system size.[41,45,46] Energy storage materials, such as Li compounds and metal hydrides, in the form of small particles or thin films transform discontinuously when wetting layers from opposing surfaces impinge.[43,47,48] This is analogous to capillary condensation[49] of vapor in small pores and not the signature of a critical-point wetting transition proper.

Atomistic models naturally include a consistent representation of the gradient energy in discrete matter. The natural, second-difference (curvature) base for the gradient energy is also allowed for in some of the plane-by-plane models,[32–34,37] which are informed by atomic-scale bond counting. Yet plane-by-plane model studies have also been based on a first-difference (gradient-) square energy,[35,36] and the gradient square is inherent to phase field models.[11,13,14,50] These gradient-square approaches invariably neglect the residuum term, $\kappa_1(\nabla x) \cdot \mathbf{n}$, of Eq. (2). In fact, none of the studies cited above addresses the term or inspects its ramifications.

Here, we provide the missing inspection of the residuum. We examine a particularly simple (minimal) example that embodies the most basic physics of critical-point wetting in solid solutions, namely a crystal with an Ising-type, nearest-neighbor bond-counting Hamiltonian, a repulsive unlike-neighbor interaction, and a composition-dependent surface energy. We use an atomistic simulation as the benchmark for a comparative discussion that explores continuum as well as discrete plane-by-plane approaches, each based alternatively on the classic gradient-square or on the Laplacian (gradient-square with residuum) of the concentration field.

Critical-point wetting provides an exemplary signature of the interactions at the crystal surface and is here studied in that sense. An in-depth examination of wetting is not the purpose of the present work.

II. ENERGY AND ITS REPRESENTATIONS

We consider a crystalline binary solution with conserved arrays of bulk and surface sites and with a composition-independent lattice parameter. The energies of the pure species in their crystalline bulk states are defined as zero, and the energy in the bulk solution is taken to arise exclusively from bonds between unlike atomic nearest neighbors, of fixed bond energy ϵ. We are interested in solutions with a miscibility gap, which emerges when $\epsilon > 0$.

A linear variation of the surface excess free energy with the composition is implemented by a broken-bond energy, $s\epsilon$, for one species only, here the solute. When the dimensionless segregation-strength parameter s is zero, pure solute and pure solvent have the same surface excess free energy, γ, whereas $s < 0$ promotes wetting of the surface of the dilute phase by the concentrated one.

The energy or enthalpy, $\mathcal{H}$, is here given by

$$\mathcal{H} = \epsilon B_{\mathrm{unlike}} + s\epsilon B_{\mathrm{broken}}, \tag{3}$$

with B_{unlike} and B_{broken} the numbers of unlike-neighbor bonds in the bulk and of superficial broken bonds originating in a solute atom, respectively. For use with phenomenological equations of state, as in Secs. IV and V below, we introduce the unlike-neighbor interaction energy parameter for the bulk,

$$\omega = Z_0\,\epsilon, \tag{4}$$

where Z_0 represents the bulk crystal lattice site coordination number.

For the Ising model of Eq. (3), the bulk alloy phase diagram depends on the crystallography but has otherwise no free parameters when specified in terms of x and of a reduced temperature variable, τ, that is scaled to the miscibility gap critical temperature (see, e.g., Ref. 51),

$$\tau = \frac{T}{T_C}. \tag{5}$$

In addition to the surface crystallographic orientation, superficial phenomena in the finite-size model's τ–x domain depend on s as the only adjustable parameter.

As a toy geometry, we consider a laterally extended, planar slab of material, bounded by free surfaces and allowing for one-dimensional composition gradients normal to the surface. In the parameter region under study, the slab is thicker than the combined widths of the near-surface gradients. This precludes capillary condensation.

We explore equilibrium states of semi-grand-canonical systems within three separate approaches. As a benchmark and the closest approximation to the equilibrium states of the model, we start out by considering the *atom-by-atom representation*. Here, equilibrium states are characterized by time-averages over instantaneous configurations generated by converged atomistic semi-grand-canonical Metropolis Monte Carlo (gcMMC) simulation on a rigid lattice. Next, we discuss the *continuum representation*, as it has been introduced in Eqs. (1) and (2) above. We point out that this representation may not have stable and energy-minimizing solutions when the gradient energy derives from the Laplacian. Stable solutions are obtained by the *plane-by-plane representation*, which considers a stack of discrete crystal planes, of quasi macroscopic lateral extension and with individual regular-solution-type equations of state. Contrary to the atomistic model, this implementation ignores (in-plane) chemical short-range order. Yet, it affords a traceable discussion of the surface boundary conditions and a simple numerical analysis of the equilibrium states.

III. ATOM-BY-ATOM REPRESENTATION

A. Procedures

The atomistic simulation implements the energy of Eq. (3) in the on-lattice gcMMC scheme described in detail in Ref. 43. In brief, the elementary event is swapping the occupancy of a randomly selected site between the two possible values, 0 or 1 for matrix- or solute-occupied, with the probability p. When the swap changes the system's energy by $\Delta\mathcal{H}$ and its net number of solute atoms by $\delta\mathcal{N}(=\pm1)$, and when the reservoir is at chemical potential m^R (see also Sec. V C below), then p is taken as

$$p = \mathrm{Min}\left[1,\ \exp\left(-\frac{\Delta\mathcal{H} - \delta\mathcal{N}\, m^R}{k_B T}\right)\right], \tag{6}$$

where k_B and T represent Boltzmann's constant and temperature, respectively.

The simulation explored a 3D, fcc crystal slab, with nearest-neighbor coordination number $Z_0 = 12$, {111}-type free surfaces and periodic boundary conditions acting in the plane. The slab contained $J = 201$ crystal planes parallel to the surface, with $M = 40\,320$ lattice sites in each plane and hence a total of $\mathcal{M}_{tot} = 8.1 \times 10^6$ sites in the slab.

The net solute fraction, $x_{tot} = \mathcal{N}_{tot}/\mathcal{M}_{tot}$ with $\mathcal{N}_{tot}$ the total amount of solute, was evaluated every $50 \times \mathcal{M}_{tot}$ successful swap events, and a state of equilibrium identified when the change in x_{tot} between two successive evaluations was $<10^{-4}$. The mean composition in each crystal plane was then computed every $\mathcal{M}_{tot}/4$ successful swap events. This was repeated for 200 times successively, and the equilibrated composition profile calculated by averaging, for each crystal plane, the 200 successive composition values. Crystal planes around the central one and with sufficiently small composition variation relative to their neighboring plane, $\Delta x < 10^{-3}$, were identified as "near-center planes." The bulk solute fraction, x_{blk}, was computed as the average composition in that set of planes.

B. Surface characteristics

We quantify the composition field near the surface by three surface-specific parameters, namely (1) the outermost-plane solute fraction x_1, (2) the specific excess Γ of solute, and (3) a wetting layer thickness t.

Γ is defined as

$$\Gamma = \frac{\mathcal{N}_{tot} - \mathcal{M}_{tot}\, x_{blk}}{M}, \tag{7}$$

and is specified in units of dense-packed solute monolayers (ML).

The wetting layer at the surface of a dilute solution may be thought of as a region of the concentrated phase of thickness t, separated from the dilute phase by an internal interface; t was estimated as

$$t = \frac{\Gamma}{\Delta x_{gap}}, \tag{8}$$

where Δx_{gap} refers to the width of the miscibility gap at the temperature in question.

C. Results

The atomistic simulation explored composition profiles at the surface of the bulk terminal dilute solution, at chemical potential $m^R = 0$. Gray circles in Fig. 1(a) display the bulk alloy phase diagram, as implied by bulk gcMMC simulations with 3D periodic boundary conditions in Ref. 43. At $2k_B T_C/\omega \sim 0.83$, the bulk critical temperature is compatible with values obtained by cluster expansion, 0.83 ± 0.01.[52] Data for x_{blk} from the present simulation (colored symbols) agree well with the results of Ref. 43.

Exemplary composition profiles, here for segregation strength parameter $s = -2/3$, in Fig. 1(b), confirm the superficial solute enrichment expected for $s < 0$. Beyond $\tau = 0.8$, a layer of the concentrated phase emerges. As the temperature increases further, that layer thickens continuously and its solute fraction decreases, in agreement with the narrowing of the bulk miscibility gap. In Fig. 1(c), the rendering of a snapshot of the equilibrated simulation box exemplifies the atomic-scale solute distribution.

Figure 2 shows additional composition profiles, at different values of τ and s. The layer thickness as well as the outermost-plane composition values vary continuously with the temperature,

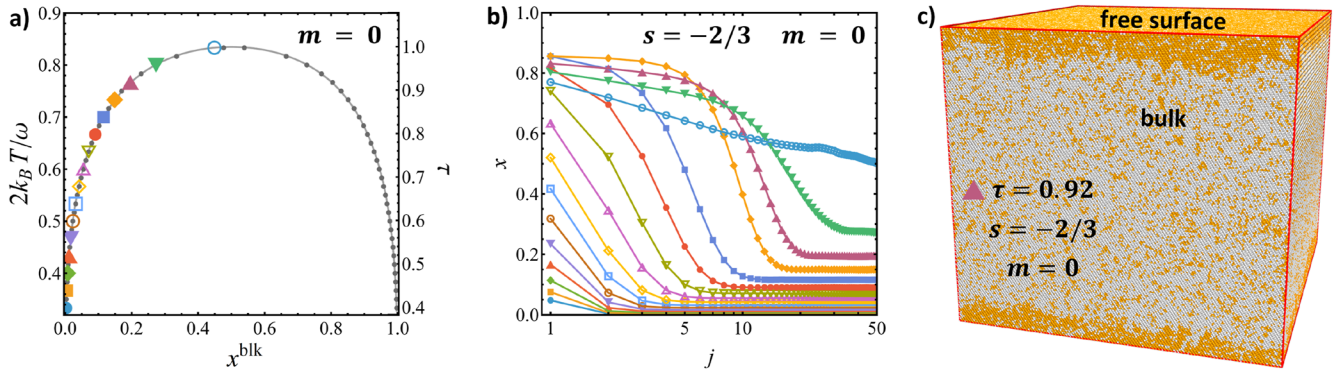

FIG. 1. Atomistic simulation–bulk alloy phase diagram and exemplary near-surface composition profiles. (a) Bulk phase diagrams showing temperature, T, normalized to solute–solute interaction energy parameter ω, vs bulk solute fraction, x_{blk}, at two-phase coexistence. Gray dots: data from Monte Carlo simulation, in Ref. 43, with 3D periodic boundary conditions; gray line: smooth interpolation as guide to the eye. Right ordinate: dimensionless temperature parameter τ. Data for $x_{blk}(\tau)$ from present work is superimposed as colored symbols. Graph serves as legend for symbol shapes and colors in (b) and in Fig. 2 below. (b) Planewise mean solute fraction x vs crystal lattice plane index j, on logarithmic scale, for τ values in panel (a). Lines: guides to the eye. (c) Rendering of snapshot from equilibrated configuration, here for $\tau = 0.92$. Gray: solvent atoms; orange: solute atoms. All data in this figure are for chemical potential $m = 0$ and segregation strength $s = -2/3$.

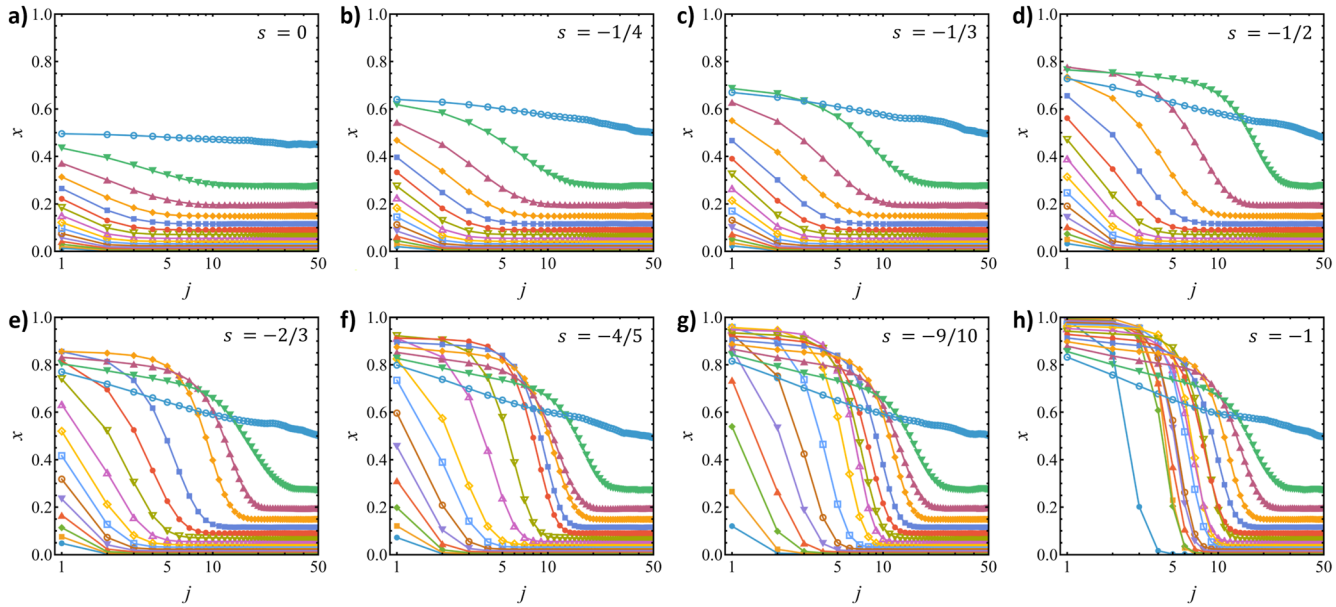

FIG. 2. Composition profiles from atomistic simulation at m = 0. (a)–(h) Planewise mean solute fraction x (symbols) vs crystal lattice plane index j, on logarithmic scale, for different values of segregation strength, s, as indicated in the graphics box headers. Scan at different reduced temperature τ; see Fig. 1(a) for legend. Lines: guides to the eye.

irrespective of the value of s. The graphs of $\Gamma(\tau)$ in Fig. 3(a) confirm this continuous increase. For the strongest segregation under study, $s = -1$, much of the increase is at very low reduced temperature, $\tau < 0.4$. That temperature regime has not been explored in our study, since wetting transitions are typically observed quite close to T_C. We also note that substantially more negative s would simply fix the outermost plane composition at $x_1 \approx 1$. For the model at hand, that "solute-saturated surface" scenario has been studied in Ref. 43. The results provided no evidence for a first-order wetting transition.

In Fig. 3(b), the graphs of $x_1(\tau)$ further illustrate the continuous evolution of the composition with temperature. The evolution of t, plotted vs $1 - \tau$ in Fig. 3(c), is also continuous at all s. For benchmark, the figure also shows the temperature-dependent Cahn–Hilliard interface width t_{CH} (see Appendix A), for the case of exclusively nearest-neighbor interaction. That latter parameter refers to the width of an internal anti-phase boundary, not a wetting layer. It serves here as a convenient reference, also illustrating the square-root variation of the interface width in the Cahn–Hilliard

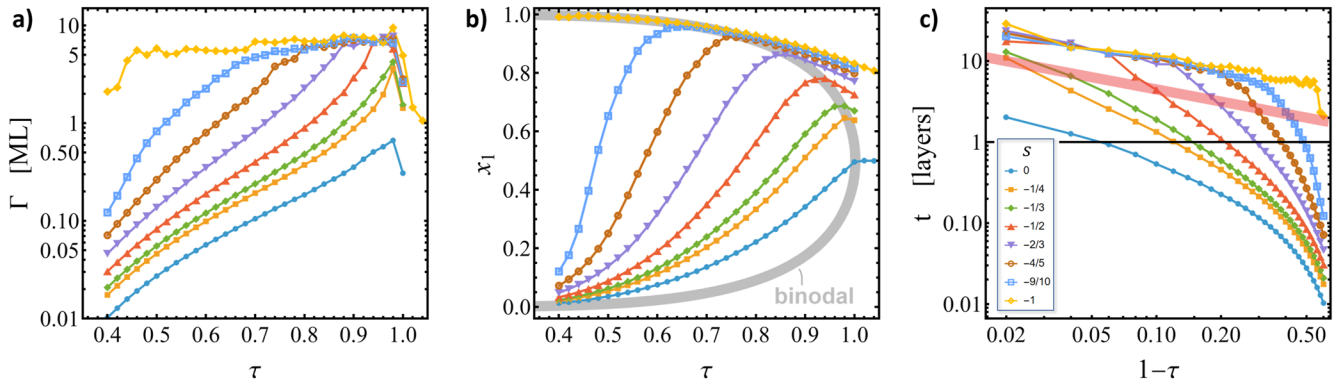

FIG. 3. Temperature scans from atomistic simulation at m = 0. (a) Specific excess, Γ, of solute; (b) outermost-plane solute fraction x_1, (c) effective wetting layer thickness, t. All parameters plotted vs the reduced temperature τ or vs $1-\tau$. Note logarithmic axis scaling for Γ, t, and $1-\tau$. See legend for values of segregation-strength parameter s. Note continuous variation of all graphs with temperature, indicating the absence of a first-order wetting transition. Thick gray line in (b) bulk binodal, for reference. Thick red line in (c) Cahn–Hilliard interface width (not a wetting layer width) as benchmark for layer thickness t.

theory. It is seen, that the effective wetting layer thickness in the approach to criticality behaves similarly to t_{CH}, with an apparent temperature exponent near 1/2. Yet, t emerges as about twice larger than t_{CH}.

In Fig. 3(a), one notes a small excess of solute even when $s = 0$. This may be understood as consequence of the lesser coordination number at the surface, which brings a reduced effective solute–solute interaction energy (Ref. 7, Sec. III.B.1). At any given temperature, the weaker interaction leads to an effectively narrowed miscibility gap at the surface, hence local compositions that are closer to 1/2 than the bulk.

In summary, the results of our atomistic simulation of the FCC Ising model with a {111} surface suggest not a first-order wetting transition but rather a continuous evolution of the near-surface composition with the temperature, with a divergence of the wetting layer thickness in the approach to the bulk critical point. Our observation is consistent with previous Monte Carlo simulations of an Ising Hamiltonian as in Eq. (18), in which no first-order wetting transition was found.[53,54]

IV. CONTINUUM REPRESENTATION

A. Semi-infinite slab with unidirectional gradient

To inspect the continuum approximation to a system with the energy of Eq. (3) at finite temperature, consider Eq. (1) for the slab with area A, normal position coordinate z, and a unidirectional composition gradient, $x = x(z)$. If we take the slab thickness as L, then,[1]

$$\frac{\mathcal{F}}{A} = \psi(x_0) + \psi(x_L) + \int_0^L \Psi(x, x', x'')\, \mathrm{d}z, \tag{9}$$

with

$$\Psi(x, x', x'') = \Psi_0(x) + \kappa_1(x)x'' + \kappa_2 x'^2, \tag{10}$$

where x_0 and x_L represent the superficial limiting values of the solute fractions and where[55]

$$\kappa_1 = \kappa_0\left(\frac{1}{2} - x\right), \quad \kappa_2 = \kappa_0, \quad \kappa_0 = \rho\omega\lambda^2, \tag{11}$$

with ρ the site density (sites per volume) and λ an effective interaction distance. Integration by parts here leads to

$$\frac{\mathcal{F}}{A} = \int_0^L \left(\Psi_0(x) + \kappa_0\, x'^2\right) \mathrm{d}z + \psi(x_0) - \kappa_1(x_0)\, x'_0 + \psi(x_L) + \kappa_1(x_L)\, x'_L. \tag{12}$$

Equations (9) and (12) are the 1D equivalents of Eqs. (1) and (2) and will be inspected in Sec. IV B below and in Appendix C. Note that these equations adopt the widely accepted[5–7,9,12,14,46] notion that the surface free energy density in continuum approaches to wetting is a function of the surface limiting value of the solute fraction, $\psi = \psi(x_S)$.

It is well established that the standard gradient-square scenario, Eq. (9) with vanishing curvature coefficient κ_1 and with short-range interactions that result in a predominantly linear $\psi(x_S)$, features a first-order wetting transition.[5–7,9,15] As pointed out in Sec. III, the first-order transition is not confirmed by the Ising model. In view of the established[1] relevance of κ_1, the discrepancy is not surprising, and it incites exploration of the continuum representation with gradient energy from the curvature (coefficient κ_1) as opposed to the gradient-square (coefficient κ_2). Yet, as we shall now expose, retaining the $\kappa_1(x)x''$ term in the continuum representation introduces a fundamental issue, which sheds doubt on the existence of stable free-energy minima for the curvature-based form of Eq. (9).

B. A trial function and the stability of solutions

While the bulk free energy term in Eq. (12) might suggest a classic problem of variational calculus, the appearance of the first derivatives in the boundary terms is not standard. Indeed, minimizing the free energy of Eq. (12) with respect to the composition profile is not a well-formed problem of variational calculus. To illustrate that issue, we find it instructive to consider the gradient energy only. Motivated by the considerations above, we tentatively take

that energy to arise exclusively from the curvature-dependent term, which scales with $\kappa_1(x)$, in Eq. (9). The gradient part of the free energy in Eq. (9) then takes the form

$$\frac{\mathcal{F}^{\mathrm{grd}}}{A} = \kappa_0 \int_0^L \left(\frac{1}{2} - x\right) x'' \mathrm{d}z. \tag{13}$$

Let us further simplify the problem by considering a semi-infinite slab ($L \to \infty$) and evaluate Eq. (13) using the following trial function for $x(z)$:

$$x = x_\infty \left(1 - \exp - \frac{z}{\Lambda}\right). \tag{14}$$

This function gives $x_0 = 0$ at the surface, and it approaches the bulk equilibrium composition, x_∞, in a gradient layer of width Λ. The energy is readily evaluated as

$$\frac{\mathcal{F}^{\mathrm{grd}}}{A} = -\frac{\kappa_0}{2\Lambda} x_\infty (1 - x_\infty). \tag{15}$$

With $0 < x < 1$, with A and $\Lambda > 0$ by definition, and with $\kappa_0 > 0$ for systems with a miscibility gap, $\mathcal{F}^{\mathrm{grd}}$ is here always negative. Thus, the gradient energy of Eq. (15) diverges to $-\infty$ as the near-surface gradient becomes ever steeper, $\Lambda \to 0$. As all other energy contributions (specifically from Ψ_0 and from ψ) will always be finite, one can find concentration profiles for which the free energy $\mathcal{F}^{\mathrm{grd}}$ of the toy problem assumes arbitrarily large negative values. These profiles may not satisfy the Euler equation, Eq. (C3) in Appendix C, yet they are energetically more favorable than all finite-energy solutions of that equation. Such solutions will then, at best, be metastable states, but they do not identify true free energy minima.

There appear to be two fundamental issues here, one related to the mathematics of curvature-based free energy expressions such as Eqs. (9) or (12), and a second related to the physical meaning of infinitely steep gradients when discussed in the context of a discrete crystal lattice.

The first fundamental issue is that the x_0', x_L' terms of the residuum in Eq. (12) lead to a set of boundary conditions for the variational problem that cannot be satisfied with the available constants of integration. In other words, the problem is over-constrained. This is exposed in detail in Appendix C.

The second fundamental issue concerns length scales. The discrete, atomic nature of matter imposes a lower limit on the spatial dimensions of variations. In contrast, the continuum theory allows for gradients at the surface in dimensions smaller than the interatomic spacing. Those gradients have no physical significance. Yet they are naturally permitted in the continuum theory, and—as just discussed—they can bring very large variations in the energy.

Numerical implementations of the continuum theory, for instance in phase-field simulation, do embody an underlying discrete length-scale in the form of the grid of materials points on which the simulation is performed; with $0 < x < 1$ they can then only represent maximum gradients in the order of the inverse grid spacing. For the curvature-energy problem, the instability against maximizing the gradient at the surface then implies that the energy of solutions will be sensitive to the grid spacing. That is again not satisfactory, because the spacing is an internal parameter of the implementation, not related to the physics of the problem.

Discrete plane-by-plane models avoid the above problem, though at the cost of restriction to one-dimensional gradients. Here, the discretization reflects the distance between crystallographic planes and, thereby, the physical scale of the discreteness of matter. The discrete representation will be considered in Sec. V below.

C. Surface free energy density function

The form of the surface free energy density function requires inspection. The physics of the interactions at the surface might warrant generalizing from $\psi = \psi(x_S)$ to $\psi = \psi(x_S, x_S', \ldots)$. One might then further envisage the special case where the x_S'-dependent contributions to ψ emerge such that they precisely cancel the residuum terms in Eq. (12). This would revert the variational problem to its standard form, which can be solved by classic approaches.

Appendix D derives ψ for the bond-counting Hamiltonian of Eq. (3), assuming regular solution behavior and dense-packed crystal planes, with interplanar spacing d_{ip}, parallel to the surface. When allowing for a linear composition gradient, ignoring higher-order derivatives, the result [see Eqs. (D4) and (D5)] is

$$\psi \propto s \left(x_S \pm \frac{d_{\mathrm{ip}}}{2} x_S'\right) - x_S(1 - x_S) - \frac{d_{\mathrm{ip}}^2}{4} (x_S')^2. \tag{16}$$

With respect to the dependency of ψ on x_S, one notes that the linear term is parameterized by the segregation strength s, consistent with a linear composition-dependence of the surface free energy. This dependency is on top of an inherent, parabolic one that reflects the reduced coordination number at the surface, as addressed in Sec. III C. The terms linear and parabolic in x_S are consistent with assumptions in continuum approaches to wetting.[5–7]

Remarkably, Eq. (16) indeed suggests a dependency of ψ also on x_S'. Yet, the linearly x_S'-dependent term in ψ scales with the surface-related parameter s and so will not generally cancel the residuum term, which is governed by independent, bulk-related parameters. The $(x_S')^2$-dependent term is negative valued, reflecting the energy gain when bonds are cut in a region of steep gradient and, hence, large gradient-square energy in the initial bulk state. Being negative, this term on its own will not counteract large gradients near surfaces.

As is apparent in Appendix D, the x_S'-dependent terms in Eq. (16) serve to extrapolate from the composition at the dividing surface of the continuum model to that in the nearest plane of the physical crystal. Thereby, the gradient terms here relate to features of the continuum model at a scale smaller than the interatomic spacing. This suggests caution in interpreting the consequences of those terms for the behavior of real crystals.

V. PLANE-BY-PLANE REPRESENTATION

A. Net energy

Our plane-by-plane representation, analogous to Refs. 33 and 34, describes the crystal as a sequence of J lattice planes, labeled $j = 1 \ldots J$, denoting by x_j the average solute fraction in plane j, and allowing for gradients in x exclusively in the direction normal to the planes. Furthermore, we take each plane as a regular solution, with solute randomly distributed over the sites in the plane.

We take M sites per plane, with M sufficiently large that significant boundary effects arise only from the free surfaces beyond $j = 1$

and $j = J$, and not from the edges of the planes. The total amount of solute is here

$$\mathcal{N}_{\rm tot} = M\sum_{j=1}^{J} x_j. \tag{17}$$

Counting bonds, one readily finds that the net energy of Eq. (3) is here

$$\begin{aligned}\mathcal{H} &= MZ_0\,\epsilon\sum_{j=2}^{J-1} x_j(1-x_j)\\ &+ MZ_\perp\,\epsilon\sum_{j=2}^{J-1}\left(\frac{1}{2}-x_j\right)(x_{j+1}-2x_j+x_{j-1})\\ &+ MZ_\parallel\,\epsilon\,[x_1(1-x_1)+x_J(1-x_J)]\\ &+ \frac{1}{2}MZ_\perp\,\epsilon\,[x_1(1-x_2)+(1-x_1)x_2]\\ &+ \frac{1}{2}MZ_\perp\,\epsilon\,[x_J(1-x_{J-1})+(1-x_J)x_{J-1}] + MZ_\perp s\,\epsilon\,[x_1+x_J].\end{aligned} \tag{18}$$

In this expression, the first line gives $\mathcal{H}$ for the uniform bulk, the second line is the correction accounting for composition gradients, and the remaining lines account for the bonding in the surface layers at $j = 1$ and J.

Equation (18) assumes nearest-neighbor bonds that extend exclusively into the immediately neighboring planes, as, for instance, in {111} or {100} planes of fcc lattices. The in-plane and (one-sided-) out-of-plane coordination numbers are denoted by $Z_\parallel$ and $Z_\perp$, respectively (e.g., $Z_\parallel = 6$ and $Z_\perp = 3$ for {111} planes in fcc). For a concise notation, we introduce

$$\zeta = Z_\perp/Z_0, \tag{19}$$

as an out-of-plane coordination parameter.

We find it useful to explicitly separate out various contributions to Eq. (18) and to express the result as

$$\mathcal{H} = \mathcal{H}^{\rm loc} + \mathcal{H}^{\rm grd} + \mathcal{H}^{\rm srf}, \tag{20}$$

the sum of local bulk, gradient, and surface terms.

We denote the energy of a crystal plane j by H_j. The per-plane energy in a region of the bulk with a uniform local environment is

$$H_j^{\rm loc} = M\omega\, x_j(1-x_j), \tag{21}$$

and the contributions of this form to the net free energy sum up to

$$\mathcal{H}^{\rm loc} = \sum_{j=1}^{J} H_j^{\rm loc}. \tag{22}$$

In the spirit of Eq. (20), the extra energy due to nonuniform composition may be specified as an excess, $H_j^{\rm grd}$, over $H_j^{\rm loc}$ at the local x_j. With Eq. (18), we find

$$H_j^{\rm grd} = -\zeta M\,\omega\left(x_j-\frac{1}{2}\right)\delta^2 x_j, \quad j = 2..\,J-1, \tag{23}$$

with δ a difference operator. Specifically, the first forward difference and the second difference operators are

$$\delta x_j = x_{j+1} - x_j, \tag{24}$$

and

$$\delta^2 x_j = x_{j+1} - 2x_j + x_{j-1} = \delta x_j - \delta x_{j-1} = \delta(\delta x)_{j-1}, \tag{25}$$

respectively. The dependence of the bulk gradient energy term, Eq. (23), on the second difference operator is a central observation here and is consistent with the discussion of the gradient energy of network solids in Ref. 1.

For the planes at the two free surfaces, Eqs. (18) and (20) imply

$$\begin{aligned}\mathcal{H}^{\rm srf} &= M\,\zeta\,\omega\left[s\,x_1 - x_1(1-x_1) - \delta x_1\left(x_1-\frac{1}{2}\right)\right]\\ &+ M\,\zeta\,\omega\left[s\,x_J - x_J(1-x_J) + \delta x_{J-1}\left(x_J-\frac{1}{2}\right)\right].\end{aligned} \tag{26}$$

The dependency of this expression on the surface layer solute fractions x_1, x_L reflects analogous terms in Eq. (16) for the surface excess free energy in the continuum representation. This concerns specifically the s-dependent linear term and the parabolic term accounting for the reduced coordination number. Furthermore, Eq. (26) includes difference terms that favor superficial solute depletion ($\delta x_1 < 0$) in dilute solutions ($1/2 - x > 0$) and enrichment in concentrated ones.

B. Summation by parts

Next, we use summation by parts to present the gradient energy contribution in the bulk as an expression involving the first instead of the second difference operator. In its natural, second-difference representation and according to Eqs. (18) and (23), the gradient contribution to $\mathcal{H}$ is

$$\mathcal{H}^{\rm grd}_{\rm 2nd} = -M\zeta\,\omega\sum_{j=2}^{J-1}\left(x_j-\frac{1}{2}\right)\delta^2 x_j. \tag{27}$$

As is shown in Appendix B, we have

$$\mathcal{H}^{\rm grd}_{\rm 2nd} = \mathcal{H}^{\rm grd}_{\rm 1st} + \mathcal{H}^{\rm res}_{\rm 1st}, \tag{28}$$

with the bulk first-difference-square term,

$$\mathcal{H}^{\rm grd}_{\rm 1st} = M\zeta\,\omega\sum_{j=1}^{J-2}(\delta x_j)^2, \tag{29}$$

and the residuum term,

$$\mathcal{H}^{\rm res}_{\rm 1st} = M\zeta\,\omega\left[\left(x_1-\frac{1}{2}\right)\delta x_1 - \left(x_{J-1}-\frac{1}{2}\right)\delta x_{J-1}\right]. \tag{30}$$

Equations (27)–(30) provide two separate representations of the identical contribution to the net energy.

Whereas the natural expression for the gradient energy, $\mathcal{H}^{\rm grd}_{\rm 2nd}$ in Eq. (27), depends on a sum over second difference operators, the new, equivalent expression involves the sum over the squares of the first difference operators, Eq. (29), supplemented by the residuum, Eq. (30), that depends on the composition and on its first differences at or near the free surfaces. This is the discrete equivalent to the integration by parts in Ref. 1.

C. Entropy and grand canonical potential

Our notion of entropy, $\mathcal{S}$, is restricted to the ideal entropy of mixing. For the regular solution, it is

$$\mathcal{S} = \sum_{j=1}^{J} S_j, \tag{31}$$

with

$$S_j = -M\,R[x_j \ln x_j + (1-x_j)\ln(1-x_j)]. \tag{32}$$

The latter expression holds for all planes, including those at the surfaces, and it is insensitive to gradients.

We allow for the system to exchange matter with an external reservoir at fixed chemical potentials for the components and a fixed number of sites. At equilibrium, the system then minimizes a semi-grand canonical potential,

$$\mathcal{O} = \mathcal{H} - T\mathcal{S} - m\,\mathcal{N}_{\mathrm{tot}}, \tag{33}$$

at $m = m^{\mathrm{R}}$. For the special case of a uniform ($x_j \equiv x$), substitutional solution with a conserved network of sites, m denotes the diffusion potential (difference of the chemical potentials, solvent minus solute); for a uniform interstitial solution, m is the chemical potential of the solute. In each case, m obeys

$$m = \frac{1}{\mathcal{M}^{\mathrm{tot}}}\frac{\mathrm{d}\left(\mathcal{H}^{\mathrm{loc}} - T\mathcal{S}\right)}{\mathrm{d}x}, \tag{34}$$

in the uniform system.

As our study aims to compare the impact of different assumptions on the gradient energy, we evaluate three specific expressions for $\mathcal{O}$, namely,

$$\mathcal{O}_{\mathrm{2nd}} = \mathcal{H}^{\mathrm{loc}} + \mathcal{H}^{\mathrm{grd}}_{\mathrm{2nd}} + \mathcal{H}^{\mathrm{srf}} - T\mathcal{S} - m\,\mathcal{N}_{\mathrm{tot}}, \tag{35}$$

$$\mathcal{O}_{\mathrm{1st}} = \mathcal{H}^{\mathrm{loc}} + \mathcal{H}^{\mathrm{grd}}_{\mathrm{1st}} + \mathcal{H}^{\mathrm{res}}_{\mathrm{1st}} + \mathcal{H}^{\mathrm{srf}} - T\mathcal{S} - m\,\mathcal{N}_{\mathrm{tot}}, \tag{36}$$

$$\mathcal{O}_{\mathrm{nrs}} = \mathcal{H}^{\mathrm{loc}} + \mathcal{H}^{\mathrm{grd}}_{\mathrm{1st}} + \mathcal{H}^{\mathrm{srf}} - T\mathcal{S} - m\,\mathcal{N}_{\mathrm{tot}}. \tag{37}$$

While Eqs. (35) and (36) are equivalent, Eq. (37) differs because it misses the residuum term.

In terms of the respective $\mathcal{O}$, the surface excess free energy, γ, (per surface atom) is obtained as

$$\gamma = \frac{1}{M}\left(\mathcal{O} - \mathcal{O}^{\mathrm{ref}}\right), \tag{38}$$

where $\mathcal{O}^{\mathrm{ref}}$ refers to the uniform bulk (no free surfaces) equilibrated with the reservoir.

D. Properties of uniform mixtures

When ω is positive valued, the interacting regular solution has a miscibility gap at the critical temperature $T_{\mathrm{C}} = \omega/(2R)$. In view of Eq. (5), the uniform regular solution has closed-form equations for the reduced binodal and spinodal temperatures,

$$\tau^{\mathrm{bin}} = (4x-2)\left(\ln\frac{x}{1-x}\right)^{-1}, \tag{39}$$

and

$$\tau^{\mathrm{spi}} = 4x(1-x), \tag{40}$$

respectively. The diffusion potential m takes the values

$$m^{\mathrm{spi}}(\tau) = \pm\omega\left(\sqrt{1-\tau} - \tau\,\mathrm{arctanh}\sqrt{1-\tau}\right), \tag{41}$$

at the spinodals.[43]

E. Numerical procedure

We have inspected equilibrium composition profiles for slabs comprising $J = 200$ planes, bounded by free surfaces. Composition profiles were enforced symmetric to a central mirror plane. Control scenarios with $J = 400$ planes provided indistinguishable results. We again studied {111}-planes of an fcc lattice, where $\zeta = 1/4$.

The numerical approach searched for local minima of the potentials of Eqs. (35)–(37), with—in view of the symmetry—$J/2$ discrete solute fractions x_j as free parameters. Fixed values were assumed for the environmental parameters τ and m^{R}, and for the segregation strength parameter s. The homogeneous dilute bulk alloy, equilibrated at the acting value of m^{R} and at the lowest τ, provided the first starting configuration. Temperature scans then used the equilibrated state at the previous temperature as the starting configuration. In this way, the temperature was scanned first upward and then back downward.

The atomistic simulation of Sec. III had explored the wetting behavior by scanning the temperature at chemical potential $m^{\mathrm{R}} = 0$, moving the system along the binodal. In the plane-by-plane representation, this approach did not reliably converge to meaningful configurations of local minimum energy, specifically at low τ and high s. The problem was traced back to the degeneracy of the energies of the coexisting phases. This results in only very small driving

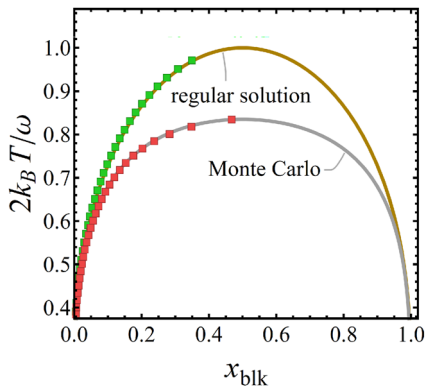

FIG. 4. Binodals and bulk composition values with a chemical potential offset. Alloy phase diagrams showing the binodals for the regular solution in the plane-by-plane model [dark yellow line, Eq (39)] and for Monte Carlo simulation results of the atomistic model (gray line; adopted from Fig. 1). Temperature, T, normalized to solute–solute interaction energy parameter ω, vs bulk solute fraction x_{blk}. Symbols: bulk composition values obtained for the respective model and chemical-potential shift parameter $o = 0.03$. Composition shifts relative to the binodals are imperceptible on the scale of the figure.

forces for displacing the internal interface after temperature change. That is problematic since the discreteness of the set of atomic planes implies a modulation, on the scale of the interplanar spacing, of the interfacial energy as the function of an effective interface position relative to the planes (see Fig. 2 in Ref. 56). Since the model has no thermal activation, the result can be erratic jumps in the interface position and, hence, in the wetting layer thickness. These jumps are an artifact of combining quasi-macroscopic free energy expressions within the planes with a discrete atomic-scale spacing. They have no equivalent in the more realistic results of our atomic-scale model. For robust results, we have shifted the system state into the stable, dilute single-phase region of the alloy phase diagram at slightly negative chemical potentials.[57] The degeneracy is then lifted, in other words, the driving force toward a uniform dilute phase in the bulk no longer vanishes.

A natural scale for the chemical potential shift is provided by m^{spi}, Eq. (41). We have shifted m away from its zero value at the binodal by a fraction, o, of the spinodal value, that is, to

$$m^{\mathrm{R}}(\tau) = -o\, m^{\mathrm{spi}}(\tau). \tag{42}$$

The o-value used below, 0.03, leaves the equilibrium bulk composition quite close to the terminal solubility. Atomistic simulation results with $o = 0.03$ are presented for comparison.

F. Composition profiles

We started out by inspecting the impact of the chemical potential offset on the bulk solute fraction x_{blk}. With $o = 0.03$, the x_{blk} in the plane-by-plane model was found to differ by not more than 1.5×10^{-3} from the respective binodal value. The shifts are imperceptible on the scale of the phase diagrams, as shown in Fig. 4.

In Fig. 4, one notes different critical temperatures between the atomistic and plane-by-plane models. This reflects that the atomistic model accounts for atomic short-range order, whereas the interacting regular solution model does not.

Next, we explored the distinction between near-surface composition profiles obtained for the plane-by-plane model with the exact expressions for $\mathcal{O}$, Eqs. (35) or (36), and with the approximate expression, Eq. (37), that ignores the residuum of Eq. (30). Figure 5 shows the comparison for two exemplary values of the segregation strength. For $s = -2/3$, the exact solution [Fig. 5(a)] has the compositions in all planes, including the outermost one, to vary continuously with τ. At low temperature, solute enrichment is confined to the outermost plane, indicating a surface segregation layer but no wetting. Upon increasing τ, the solute-enriched region thickens and thus continuously evolves into a wetting layer. This is qualitatively consistent with the findings from the atomistic model (Fig. 2), supporting the absence of a first-order wetting transition.

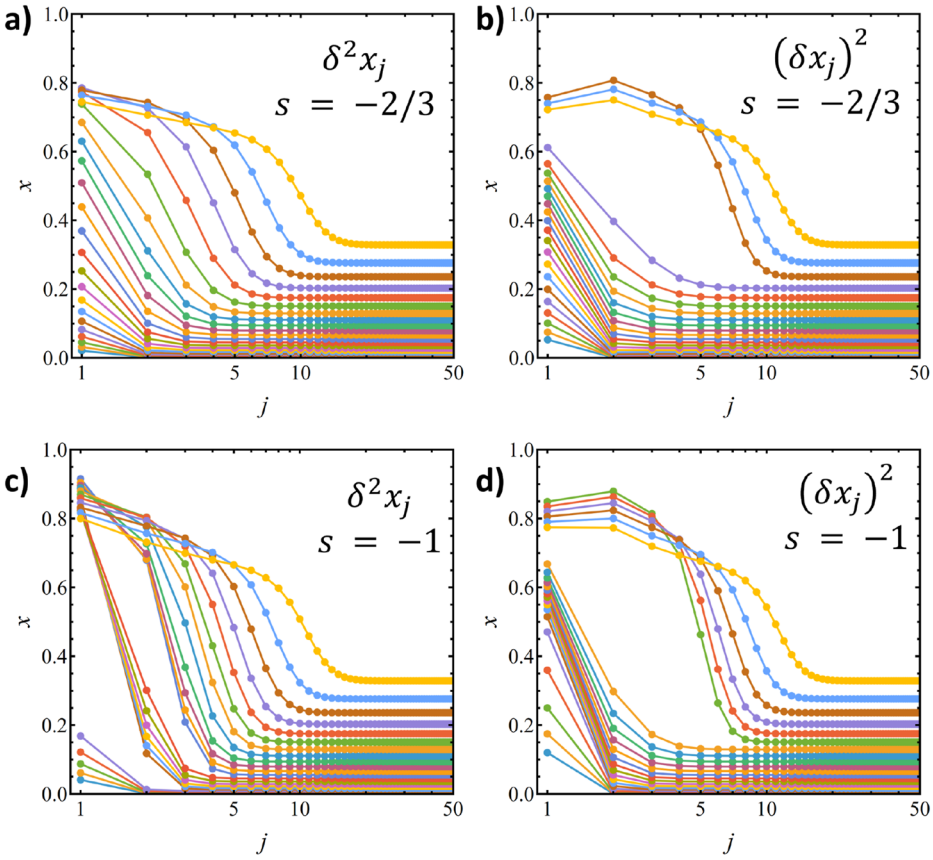

FIG. 5. Near-surface composition profiles in the plane-by-plane model: comparing exact, second-difference based solution to first-difference-square one ignoring the residuum. Solute fraction x vs layer index j, on logarithmic scale, as the temperature moves upward in 21 equidistant steps between $\tau = 0.3$ (blue disks at bottom) to 0.98 (yellow disks near top). Top row, (a) and (b) segregation strength parameter $s = -2/3$. Bottom row, (c) and (d) $s = -1$. Left column: numerical solution of the exact problem in its second-difference formulation, Eq. (35). Right column: approximate solution, Eq. (37), based on the first-difference-square description and ignoring the residuum. In top row, note continuous evolution of composition profile in panel (a) but jump, suggestive of first-order wetting transition, in panel (b). For discussion of bottom row, see the main text. All results are for chemical-potential offset parameter $o = 0.03$.

As compared to the exact solution, the approximate one [Fig. 5(b)] shows a qualitatively different behavior. For $\tau > 0.875$, the sign of the gradient between first and second crystal plane is inverted. Even more remarkably, the near-surface composition profile here exhibits a jump, from localized enrichment in the outermost layer to a several-layer-thick region of the concentrated phase. This is the characteristic of a first-order wetting transition. Yet, comparison with the atomistic model and with the exact solution of the plane-by-plane model qualifies this transition as an artifact of the approximation.

The panels in the bottom row of Fig. 5 explore a somewhat stronger segregation strength, $s = -1$. Here, the exact solution is also discontinuous. At around $\tau = 0.45$, the outermost-plane solute fraction jumps to values characteristic of the concentrated phase. The jump is again confined to the outermost plane. A second transition, near $\tau = 0.62$, has the subsurface layer also jump to the composition of the concentrated phase. The transitions remain confined to the two outermost planes, while the underlying bulk retains the composition of the dilute phase. Thereby, they appear as the signatures of localized surface phase transitions, in other words, they suggest complexions[58,59] rather than wetting transitions. Yet, here again, the features of the plane-by-plane model have no equivalent in the atomistic simulation results, thus the complexions must be rejected as artifacts.

G. Temperature-dependent characteristics

We now consider the temperature dependence of surface characteristics, starting out with the specific surface free energy γ. First, we have carefully verified that the two nominally equivalent expressions, Eqs. (35) or (36), for the exact free energy of the plane-by-plane model indeed provide identical numerical results. This is demonstrated by the superimposed results for $\gamma(\tau)$ (blue and orange disks) in Figs. 6(a) and 6(b). Further examples can be found in Figs. 6(c) and 6(d) and in Fig. 7 below.

Panels (a) and (b) in Fig. 6 show $\gamma(\tau)$ for the example of $s = -2/3$. Data for the approximate solution of Eq. (37) are superimposed to the exact solution. The approximate γ differs by exhibiting, at all nonzero s, temperature intervals with two separate branches. This feature of the approximate solution confirms its first-order wetting transition, consistent with what is implied by the composition profiles of Figs. 5(b) and 5(d). Here again, the approximate result is not supported by the exact solution, which exhibits a single branch of $\gamma(\tau)$. This confirms that the wetting transition of the approximate solution is an artifact.

Panels (c) and (d) in Fig. 6 compare temperature-dependent surface tensions for the exact and approximate solutions, respectively, with different segregation strength parameter values. For all nonzero s, the graphs of the approximate γ exhibit intervals with two branches, consistent with what was just discussed. An interesting observation, in Fig. 6(c), is the branching also in the exact solution, here for $s \leq -0.9$. This connects to our discussion of the jumps in the outermost two planes, see Fig. 5 above, which we had qualified as artifacts. Our discussion in Sec. V E links the artifact to the plane-by-plane model's combination of the atomic-scale, out-of-plane discreteness with a quasi-macroscopic free energy expression within each plane.

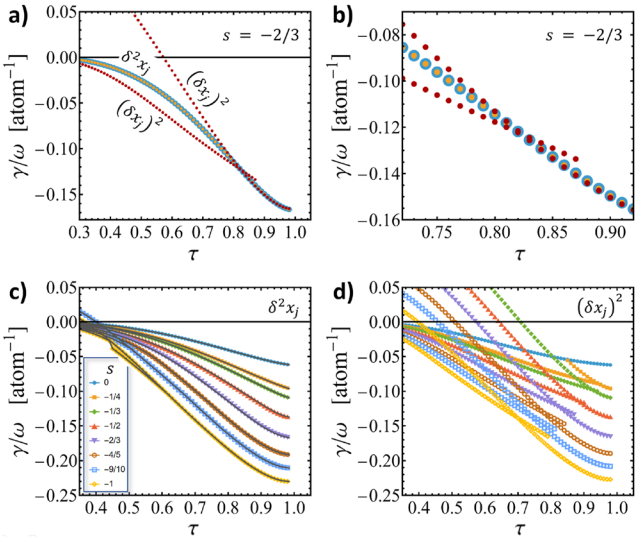

FIG. 6. Temperature variation of specific surface excess free energy γ in the plane-by-plane model. (a) Overview showing superposition of γ, normalized to solute–solute interaction parameter ω, vs dimensionless temperature variable τ, for up- and then down scans in τ. Bold blue and narrow yellow disks: exact, second-difference based solutions as represented by Eqs. (35) and (36), respectively. Note excellent mutual agreement. Red symbols: approximate solution of Eq. (37), based on the first-difference square and ignoring the residuum; note large and qualitative deviation from the exact solution. Segregation strength parameter $s = -2/3$. (b) Detail from (a), showing crossing of two $\gamma(\tau)$ branches of the approximate solution, suggestive of a first-order transition, which has no equivalent in the exact solution. (c) $\gamma(\tau)$ of the exact solution, for different s (see legend). Colored symbols and black lines represent Eqs. (35) and (36), respectively. Note continuous graphs (except for branching at the two highest s values), suggesting absence of surface phase transition. (d) As in panel (c), but for approximate solution, Eq. (37). Note two intersecting branches at all nonzero s values. All results are for chemical-potential offset parameter $o = 0.03$.

Figure 7 compares the results of the plane-by-plane representation (exact or approximate) among themselves and with the benchmark computation for the atomistic representation. Here again, all panels use a chemical-potential offset parameter $o = 0.03$.

Panels (a)–(c) of Fig. 7 show the results of our benchmark, the atomistic model, here with the chemical-potential offset. Comparison to the results for $m = 0$, without offset, in Fig. 3 reveals that the increase of Γ with τ is now more gradual. That being said, the present atomistic results are qualitatively consistent with all conclusions from the $m = 0$ scenario. This suggests that meaningful conclusions can be obtained by discussing the plane-by-plane model results obtained with the chemical potential offset.

Panels (d)–(f) of Fig. 7 show results for the exact solution of the plane-by-plane model. The graphs agree qualitatively with those of the atomistic model, except that the wetting layer near T_C is here thinner and that complexions appear at $s = -0.9$ and -1. The complexions emerge not as singular observations, but instead humps in the graphs of all three quantities appear already at weaker segregation strength. The remaining aspects of the two approaches, atomistic and (exact) plane-by-plane, are remarkably consistent. Most importantly, the exact solution of the plane-by-

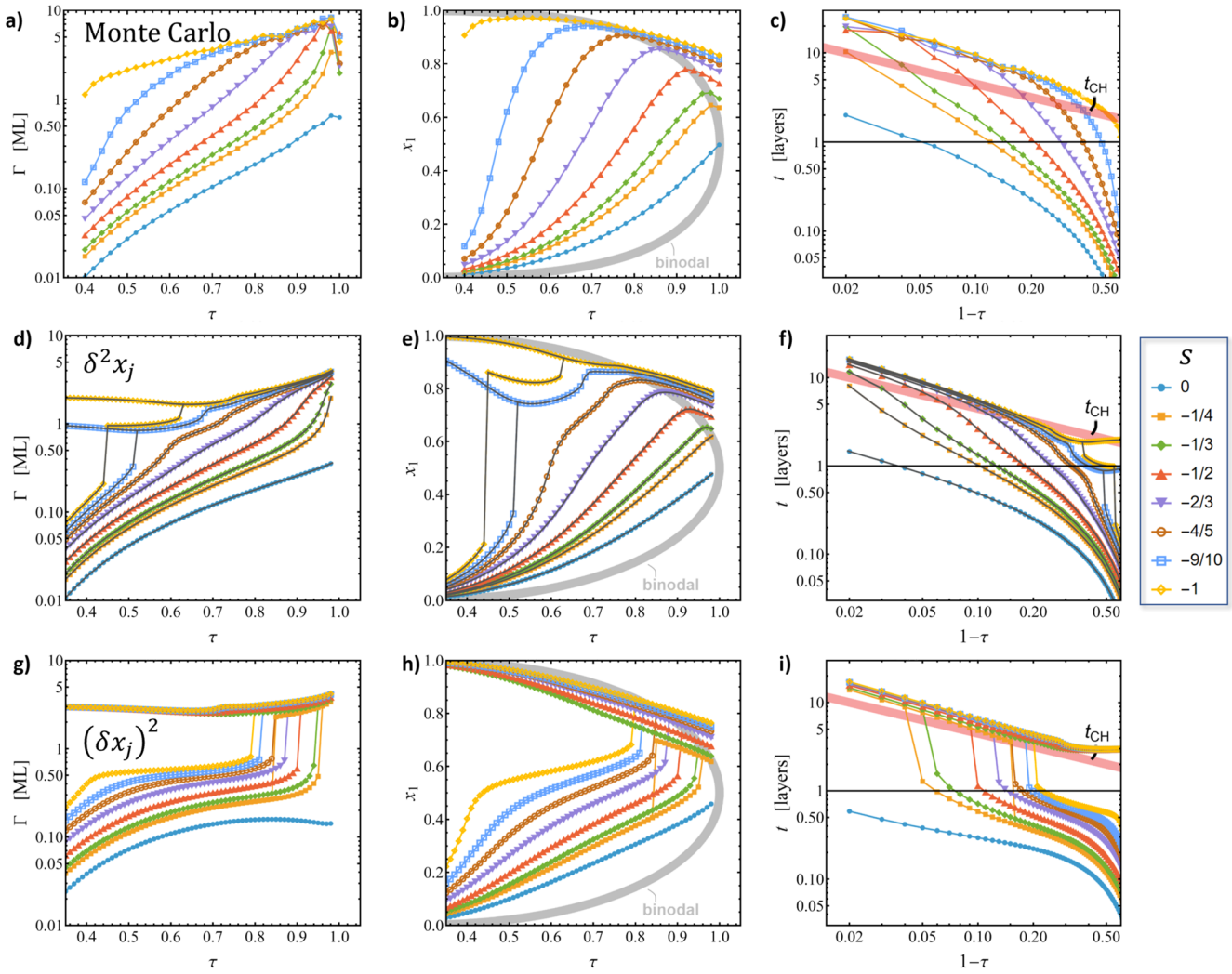

FIG. 7. Temperature variation of interfacial parameters for systems with the bulk composition near the dilute binodal—comparing different approaches. Graphs show specific excess, Γ, of solute, first-plane solute fraction x_1, and effective wetting layer thickness, t, plotted vs the reduced temperature τ or vs $1-\tau$. Note logarithmic axis scaling for Γ, t, and $1-\tau$. All results are for chemical-potential offset parameter $o = 0.03$. Top row, (a)–(c) atomistic simulation. Center row, (d)–(f) plane-by-plane model exact solution (symbols: second-difference representation; lines: first-difference-square representation including the residuum). Bottom row, (g)–(j) plane-by-plane model approximate solution, ignoring the residuum. See the legend for values of segregation-strength parameter s. Note first-order wetting transitions to several-plane-thick surface phase in approximate description, vs gradual thickening or single-plane jump in exact description. Thick red line: Cahn–Hilliard interface width t_{CH} (not a wetting layer width) as benchmark for layer thickness t.

plane model correctly reproduces the continuous variation of the wetting-layer thickness upon the approach to the bulk critical temperature. Thereby, this model correctly transports the absence of a first-order wetting transition. The previously published second-difference studies[32] indeed find no first-order wetting transition for {111} free surfaces, in agreement with our results, whereas previously published first-difference-square studies do find the first order transition—again in agreement with our results.[35,36]

Note that Fig. 7(d) confirms the small excess of solute even when the segregation strength is zero, as observed in our atomistic model and discussed there (see Sec. III C) as an effect of the parabolic part of $\psi(x_S)$ in Eq. (16).

Panels (g)–(j) present the analogous results for the approximate solution of the plane-by-plane model, ignoring the Cahn–Hilliard residuum. These results do suggest first-order wetting transitions, as evidenced by discontinuous jumps from $t \lesssim 1$ layer to $t \gg 1$ layer at well-defined temperatures. The transitions are seen to move closer to the bulk critical temperature as the segregation strength decreases. At first sight, that result is reasonable, since a smaller perturbation at the surface will only become relevant closer to criticality. Yet, in view

of the smooth $t(\tau)$ of the exact solution, and recalling our previous discussion, the prediction of a transition must again be discarded as an artifact from the omission of the residuum.

VI. DISCUSSION AND CONCLUSIONS

Our analysis explores the distinction between gradient-square-based and Laplacian-based excess energy terms near surfaces of nonuniform solid solutions, as it emerges from the 1958 analysis by Cahn and Hilliard. As a toy problem for illustration, we consider equilibrium states of the fcc Ising model with {111} surfaces and a composition-dependent surface energy. Three approaches to the free-energy minimization for that model are compared, namely (i) atomistic Metropolis Monte Carlo simulation, (ii) a regular solution plane-by-plane model, and (iii) a continuum representation.

The atomistic approach works with a rigid lattice, and the plane-by-plane as well as continuum representations ignore pressure-dependent contributions to the chemical potential. This approximation is appropriate for equilibrium states on an extended coherent lattice, provided that the interaction parameters ϵ and ω are identified with the "chemical" contribution to the interaction energy, ignoring the misfit strain energy contribution.[43,48,60]

The atomistic simulation is set up to provide an exact (except for numerical error) solution of temperature-dependent mean composition profiles in the scenario at hand. The simulation finds continuous wetting, that is, a wetting layer thickness that increases continuously with temperature, diverging as the bulk critical temperature is approached along the binodal. A first-order wetting transition can be excluded.

In coarse-grained representations derived from the Ising model, unidirectional gradients in the solute fraction affect the energy through the second derivative or the second-difference operator. We argue that the Cahn–Hilliard continuum model, when accounting for the second derivative or, equivalently, when including the residuum, has no stable and physically meaningful solutions for scenarios including free surfaces. At the heart of the issue is the failure of the continuum representation to account for the restrictions, as they are imposed by the discrete nature of atomic matter, on the magnitude of composition gradients.

The plane-by-plane model accounts for the discrete atomic structure in the direction of a 1D gradient normal to the surface. When adopting the second-difference-based formulation, the model qualitatively reproduces the findings from the atomistic simulation, and specifically continuous wetting rather than a first-order wetting transition.

As an exception to the above statement, the plane-by-plane model suggests, for large segregation strength, transitions confined to the two outermost crystal planes near the surface—in other words, complexions. The complexions are not confirmed by the atomistic model. They may be explained as artifacts from the combination of a quasi-macroscopic free energy expression within each plane with a discrete, atomic scale stacking sequence along the normal.

Summation by parts supplies a formulation of the plane-by-plane model that works with the first-difference square and that provides identical results. Remarkably, a first-order wetting transition does appear when, in an approximate version of that model, the residuum from the summation by parts is omitted. This demonstrates that the distinction between curvature-derived vs gradient-square-derived energy expressions entails qualitatively different predictions on the wetting behavior. In view of their disagreement with the atomistic results, the predictions from the approximate version of the plane-by-plane model must be rated as incorrect.

One might speculate whether the instability of the curvature-based continuum model can be removed when the continuum treatment of the bulk is supplemented with a surface term that accounts for the discrete atomic nature of the outermost plane at the surface. This might be implemented by a local composition jump at the surface as an extra parameter, similar to local displacement jumps in the continuum theory of surface mechanics.[61] Yet, testing this hypothesis by finding and validating a consistent and convincing implementation is beyond the scope of the present work.

It is well established that critical-point wetting phenomena depend sensitively on the nature of the molecular interactions. From a wide range of possible scenarios, our study focuses on the Ising model as a convenient framework to examine the distinction between gradient-square and Laplacian-based excess energy terms in solid solutions. We emphasize that fluid mixtures exhibit fundamentally different behavior. Unlike network solids, fluids are characterized by molecular rearrangements and continuously evolving local environments, allowing them to explore configuration space in closer agreement with continuum descriptions. Accordingly, continuum approaches—as pioneered by[5]—are well known to achieve excellent agreement with experiments on critical-point wetting in fluids.

In contrast to fluids, continuum approaches can be problematic for the free-energy minimization near surfaces of solids. When the concentration field is known, the free energy is here governed by the Laplacian, rather than the gradient square.[1] However, a Laplacian-based free-energy functional that includes a free surface does not readily admit meaningful energy minimization by standard variational methods for finding unknown concentration fields. Discrete approaches, such as numerical analysis of plane-by-plane models, do yield energy-minimizing concentration profiles in qualitative agreement with atomistic simulation. Yet these methods are typically restricted to unidirectional gradients, and they rely on simplified equations of state, such as the regular solution model. Ultimately, the choice between Laplacian and gradient-square formulations alters the predicted order of the phase transformation, underscoring the fundamental importance of this distinction.

ACKNOWLEDGMENTS

An early approach to the present topic was the subject of a discussion meeting between John W. Cahn, Geoffrey McFadden, and Jörg Weissmüller at NIST in 2006. Specifically, the concepts of Secs. IV A, IV B, and Appendix C of this work were developed in that round. We thank Geoffrey McFadden for permission to include those insights. This work was supported by Deutsche Forschungsgemeinschaft as part of the Excellence Strategy of the Federal Government and the federal states - EXC 3120/1 BlueMat: Water-Driven Materials - 533771286.

AUTHOR DECLARATIONS

Conflict of Interest

The authors have no conflicts to disclose.

Author Contributions

Marine Bossert: Conceptualization (supporting); Formal analysis (lead); Funding acquisition (lead); Investigation (equal); Methodology (equal); Validation (equal); Writing – original draft (equal); Writing – review & editing (equal). **Yong Li**: Conceptualization (supporting); Investigation (equal); Methodology (equal); Validation (equal); Writing – original draft (equal); Writing – review & editing (equal). **Jörg Weissmüller**: Conceptualization (lead); Formal analysis (lead); Funding acquisition (lead); Investigation (equal); Methodology (equal); Validation (equal); Writing – original draft (lead); Writing – review & editing (equal).

DATA AVAILABILITY

The data that support the findings of this study are available from the corresponding author upon reasonable request.

APPENDIX A: CAHN–HILLIARD INTERFACE WIDTH

The main text refers to the Cahn–Hilliard interface width, t_{CH}, as a benchmark for the wetting layer thickness. Cahn and Hilliard[1] introduce an effective interaction distance λ and find

$$\lambda = \frac{r_0}{\sqrt{3}}, \tag{A1}$$

for the nearest-neighbor interaction scenarios that are of interest in the present work. Here, r_0 refers to the atomic nearest-neighbor spacing. In terms of that parameter, they find the antiphase boundary width as

$$t_{\mathrm{CH}} = 2\lambda \sqrt{\frac{1}{1-\tau}}, \tag{A2}$$

asymptotically in the approach to the critical point.

Consistent with the numerical examples studied here, we may refer to the interplanar spacing by d and assume dense-packed $\{111\}$-planes in a phase-centered cubic lattice, where $r_0 = \sqrt{3/2}\, d$ and, hence,

$$\lambda = d/\sqrt{2}. \tag{A3}$$

In our dimensionless scenario with $d = 1$, we then have $\lambda = 1/\sqrt{2}$ and, consequently,

$$t_{\mathrm{CH}} = \sqrt{\frac{2}{1-\tau}}. \tag{A4}$$

That equation is plotted as a benchmark line in our graphics showing the wetting-layer width vs $1 - \tau$.

APPENDIX B: SUMMATION BY PARTS

The summation by parts acts on the gradient energy term in second-difference representation, Eq. (27). For conciseness of notation, we introduce the composition parameter $\xi = x - 1/2$, in terms of which that equation reads

$$\mathcal{H}^{\mathrm{grd}} = -M\zeta\, \omega \sum_{j=2}^{J-1} \xi_j\, \delta^2 \xi_j. \tag{B1}$$

In view of the definitions of the difference operators, the sum can be transformed by the following sequence of steps:

$$\begin{aligned}
\sum_{j=2}^{J-1} \xi_j\, \delta^2 \xi_j &= \sum_{j=2}^{J-1} \xi_j\, \delta(\delta\xi)_{j-1} \\
&= \sum_{j=2}^{J-1} (\xi_j - \xi_{j-1})\, \delta(\delta\xi)_{j-1} + \sum_{j=2}^{J-1} \xi_{j-1}\, \delta(\delta\xi)_{j-1} \\
&= \sum_{j=2}^{J-1} \delta\xi_{j-1}\, \delta(\delta\xi)_{j-1} + \sum_{j=2}^{J-1} \xi_{j-1}\, \delta(\delta\xi)_{j-1} \\
&= \sum_{j=1}^{J-2} \delta\xi_j\, \delta(\delta\xi)_j + \sum_{j=1}^{J-2} \xi_j\, \delta(\delta\xi)_j.
\end{aligned} \tag{B2}$$

At this point, we take recourse to Abel's summation-by-parts formula (Ref. 62, Sec. 2.4.2), in its form

$$\sum_{k=m}^{n} b_k \delta x_k + \sum_{m}^{n} x_{k+1} \delta b_k = b_{n+1} x_{n+1} - b_m x_m. \tag{B3}$$

This here implies

$$\sum_{j=1}^{J-2} \xi_j \delta(\delta\xi)_j = -\sum_{j=1}^{J-2} \delta\xi_{j+1} \delta\xi_j + \xi_{J-1}\delta\xi_{J-1} - \xi_1 \delta\xi_1. \tag{B4}$$

Using that result for replacing the second term on the right in the last line of Eq. (B2), the sequence of manipulations there may be continued as

$$\begin{aligned}
\sum_{j=2}^{J-1} \xi_j\, \delta^2 \xi_j &= \sum_{j=1}^{J-2} \delta\xi_j\, \delta(\delta\xi)_j - \sum_{j=1}^{J-2} \delta\xi_{j+1}\delta\xi_j + \xi_{J-1}\delta\xi_{J-1} - \xi_1\delta\xi_1 \\
&= \sum_{j=1}^{J-2} \delta\xi_j\, (\delta\xi_{j+1} - \delta\xi_j) - \sum_{j=1}^{J-2} \delta\xi_{j+1}\delta\xi_j + \xi_{J-1}\delta\xi_{J-1} - \xi_1\delta\xi_1 \\
&= -\sum_{j=1}^{J-2} (\delta\xi_j)^2 + \xi_{J-1}\delta\xi_{J-1} - \xi_1\delta\xi_1.
\end{aligned} \tag{B5}$$

The last equation in Eq. (B5) completes the partial summation. Converting back from ξ to x as the composition parameter and summarizing, we see that

$$\begin{aligned}
&-M\zeta\, \omega \sum_{j=2}^{J-1} \left(x_j - \frac{1}{2}\right) \delta^2 x_j \\
&\quad = M\zeta\, \omega \left[\sum_{j=1}^{J-2} (\delta x_j)^2 + \left(x_1 - \frac{1}{2}\right)\delta x_1 - \left(x_{J-1} - \frac{1}{2}\right)\delta x_{J-1}\right],
\end{aligned} \tag{B6}$$

which summarizes Eqs. (27)–(30) of the main text.

APPENDIX C: BOUNDARY CONDITIONS

Consider the free energy $\mathcal{F}$ of Eq. (12) in the main text. The condition of minimum $\mathcal{F}$ can be written as

$$0 = \frac{\delta \mathcal{F}}{A} = \int_0^L \left(\Psi_0'(x)\delta x + 2\kappa_0 x' \delta x'\right) \mathrm{d}x + \left(\psi_0' - \kappa_1' x_0'\right)\delta x_0 + \left(\psi_L' + \kappa_1' x_L'\right)\delta x_L - \kappa_1(x_0)\delta x_0' + \kappa_1(x_L)\delta x_L'. \quad \text{(C1)}$$

Partial integration gives

$$0 = \int_0^L \left(\Psi_0'(x) - 2\kappa_0 x''\right)\delta x \ \mathrm{d}x + \left(\psi_0' - \left(\kappa_1' + 2\kappa_0\right)x_0'\right)\delta x_0 + \left(\psi_L' + \left(\kappa_1' + 2\kappa_0\right)x_L'\right)\delta x_L - \kappa_1(x_0)\delta x_0' + \kappa_1(x_L)\delta x_L'. \quad \text{(C2)}$$

By considering only variations for which δx as well as $\delta x'$ vanish at the surface, one obtains the Euler equation,

$$\Psi_0'(x) = 2\kappa_0 x'', \quad \text{(C3)}$$

which, upon first integration, gives[5]

$$\Psi_0(x) = \kappa_0 x'^2 + \eta, \quad \text{(C4)}$$

with η an integration constant.

The standard approach toward minimizing $\mathcal{F}$ of Eq. (12) is to consider next variations for which δx but not $\delta x'$ vanish at the boundaries, and finally general variations. This supplies four boundary conditions,

$$0 = \psi_0' - \left(\kappa_1' + 2\kappa_0\right)x_0', \quad \text{(C5)}$$

$$0 = \psi_L' + \left(\kappa_1' + 2\kappa_0\right)x_L', \quad \text{(C6)}$$

$$0 = \kappa_1(x_0), \quad \text{(C7)}$$

$$0 = \kappa_1(x_L). \quad \text{(C8)}$$

It is readily seen that the set of equations, Eq. (C3) with Eqs. (C5)–(C8), does not represent a well-formed variational problem: the two constants of integration which can be specified for the second order differential equation, Eq. (C3), do not generally allow to satisfy all four boundary conditions, Eqs. (C5)–(C8). This agrees with the observation that–in view of Eq. (11)(1)–Ψ of Eq. (10) in the main text does not generally satisfy the appropriate version of the Legendre condition of variational calculus,

$$\frac{\partial^2 \Psi}{\partial x'^2} > 0. \quad \text{(C9)}$$

APPENDIX D: SURFACE FREE ENERGY DENSITY FUNCTION IN THE PRESENCE OF A LINEAR COMPOSITION GRADIENT

We are interested in how the surface free energy density at a planar crystal surface is affected by a composition gradient $x_S\prime$. To this end, we consider an extended crystal, formed by a stack of lattice planes indexed j and with mean solute fractions x_j, that form an arbitrary, but fixed 1D composition profile. A continuous function $x(z)$ interpolates the composition variation in the crystal, which we take to be bounded by outer surfaces at $z = -L$ to L. Assuming uniform composition near those surfaces, and ignoring their surface free energy densities for conciseness, the continuum representation of Sec. IV A yields the free energy of the initial, extended crystal as

$$\frac{\mathcal{F}}{A} = \int_{-L}^{+L} \left(\Psi_0(x) + \kappa_1 \ x''\right) \mathrm{d}z = \int_{-L}^{+L} \left(\Psi_0(x) + \kappa_0 \ (x')^2\right) \mathrm{d}z. \quad \text{(D1)}$$

Now let the crystal be bisected at an arbitrary internal position with a composition gradient, far from the outer surfaces. The bisection between lattice planes indexed j^- and j^+ generates two half-crystals with two new surfaces. The dividing surface of the continuum description is naturally located halfway between the two surface lattice planes; see illustration in Fig. 8.

Within a regular solution model with the Hamiltonian of Eq. (3), the physical process of bisection changes the free energy (exclusively) by breaking all bonds that cross the surface. In view of Eq. (3), this extra energy is

$$\delta \mathcal{F} = \epsilon\left(\delta B_{\text{unlike}} + s\ \delta B_{\text{broken}}\right). \quad \text{(D2)}$$

Denoting the mean solute fractions of the surface lattice planes by x^- and x^+, one readily finds the loss of unlike neighbor bonds as $\delta B_{\text{unlike}} = -\rho_S Z_\perp A\left(x^-(1-x^+) + x^+(1-x^-)\right)$ and the gain in broken bonds as $\delta B_{\text{broken}} = +\rho_S Z_\perp A\left(x^- + x^+\right)$, with ρ_S the area density of sites in a lattice plane.

$\delta\mathcal{F}/A$ can be identified with the sum of the surface free energy densities, ψ^- and ψ^+, of the two newly created surfaces. Expressing

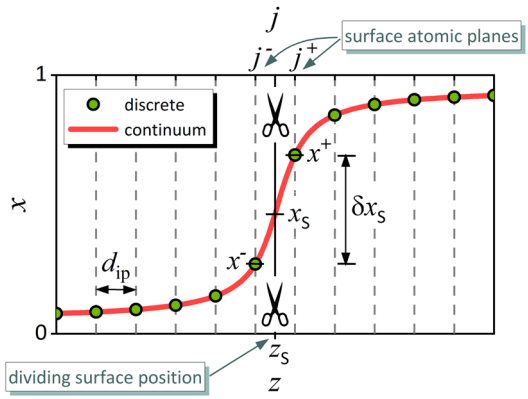

FIG. 8. Composition variation near a surface generated by bisecting an extended crystal with a 1D composition profile. Solute fraction x vs crystal lattice plane index j (top axis and circles) in the discrete representation and vs the continuous position coordinates z (bottom axis and red line) in the continuum representation. A surface is generated by bisecting between the two neighboring lattice planes j^- and j^+ (which then form the surface atomic planes), with the continuum-model's dividing surface located halfway in-between, at $z = z_S$. Symbols denote the following: x^- and x^+, solute fractions in the surface atomic planes; δx_S, composition jump across the dividing surface; x_S, surface solute fraction in the continuum representation; d_{ip}, interplanar spacing.

the ψ by the parameters of the continuum model requires that x^- and x^+ be replaced with the solute fraction, x_S, at the dividing surface and with the composition gradient, x'_S, there. As illustrated in Fig. 8, this is achieved by substituting

$$x^- \to x_S - \frac{1}{2}\delta x_S, \qquad x^+ \to x_S + \frac{1}{2}\delta x_S, \tag{D3}$$

where δx_S denotes the composition jump between the two surface planes. In a small-gradient approximation, δx_S may be expressed in terms of the continuum representation's composition gradient, x'_S, at the dividing surface and of the interplanar spacing, d_{ip}, through $\delta x_S = d_{ip} x'_S$. With the substitution and the approximation, the surface free energy densities emerge as

$$\psi^- = \rho_S \zeta \omega \left(s\left(x_S - \frac{d_{ip}}{2} x'_S \right) - x_S(1 - x_S) - \frac{d_{ip}^2}{4} (x'_S)^2 \right), \tag{D4}$$

and

$$\psi^+ = \rho_S \zeta \omega \left(s\left(x_S + \frac{d_{ip}}{2} x'_S \right) - x_S(1 - x_S) - \frac{d_{ip}^2}{4} (x'_S)^2 \right). \tag{D5}$$

It is seen that the surface free energy functions are of the form $\psi = \psi(x_S, x'_S)$.

In view of Eqs. (12) and (D1), the free energy of a crystal—here for the example of the right-hand-side crystal, labeled "+", and again ignoring the surface free energy density at the $z = L$ surface —with a composition gradient at one of its surfaces is obtained as

$$\begin{aligned} \frac{\mathcal{F}}{A} &= \int_{z_S}^{L} \left(\Psi_0(x) + \kappa_1 \, x'' \right) \mathrm{d}z + \psi^+(x_S, x'_S) \\ &= \int_{z_S}^{L} \left(\Psi_0(x) + \kappa_0 \, (x')^2 \right) \mathrm{d}z - \kappa_1(x_S) x'_S + \psi^+(x_S, x'_S). \end{aligned} \tag{D6}$$

In Eq. (D6), the coefficients determining κ_1 [Eq. (11)] and ψ^+ [Eq. (D5)] are such that the dependencies on the surface gradient terms will, as a rule, not mutually cancel.

REFERENCES

[1] J. W. Cahn and J. E. Hilliard, "Free energy of a nonuniform system 1. Interfacial free energy," J. Chem. Phys. **28**, 258–267 (1958).
[2] W. J. Boettinger, J. A. Warren, C. Beckermann, and A. Karma, "Phase-field simulation of solidification," Annu. Rev. Mater. Res. **32**, 163–194 (2002).
[3] L.-Q. Chen, "Phase-field models for microstructure evolution," Annu. Rev. Mater. Res. **32**, 113–140 (2002).
[4] I. Steinbach, "Phase-field models in materials science," Modell. Simul. Mater. Sci. Eng. **17**, 073001 (2009).
[5] J. W. Cahn, "Critical-point wetting," J. Chem. Phys. **66**, 3667–3672 (1977).
[6] H. Nakanishi and M. E. Fisher, "Multicriticality of wetting, prewetting, and surface transitions," Phys. Rev. Lett. **49**, 1565 (1982).
[7] P.-G. de Gennes, "Wetting: Statics and dynamics," Rev. Mod. Phys. **57**, 827 (1985).
[8] S. Dietrich, "Wetting phenomena," in *Phase Transitions and Critical Phenomena*, edited by C. Domb and J. L. Lebowitz (Academic Press, London, 1988), Vol. 12, pp. 1–218.
[9] J. O. Indekeu, K. Ragil, D. Bonn, D. Broseta, and J. Meunier, "Wetting of alkanes on water from a Cahn-type theory: Effects of long-range forces," J. Stat. Phys. **95**, 1009–1043 (1999).
[10] D. Bonn and D. Ross, "Wetting transitions," Rep. Prog. Phys. **64**, 1085 (2001).
[11] C. M. Bishop, M. Tang, R. M. Cannon, and W. C. Carter, "Continuum modelling and representations of interfaces and their transitions in materials," Mater. Sci. Eng.: A **422**, 102–114 (2006).
[12] M. Tang, W. C. Carter, and R. M. Cannon, "Diffuse interface model for structural transitions of grain boundaries," Phys. Rev. B **73**, 024102 (2006).
[13] Y. Mishin, W. J. Boettinger, J. A. Warren, and G. B. McFadden, "Thermodynamics of grain boundary premelting in alloys. I. Phase-field modeling," Acta Mater. **57**, 3771–3785 (2009).
[14] F. Wang and B. Nestler, "Wetting transition and phase separation on flat substrates and in porous structures," J. Chem. Phys. **154**, 094704 (2021).
[15] D. Bonn, J. Eggers, J. Indekeu, J. Meunier, and E. Rolley, "Wetting and spreading," Rev. Mod. Phys. **81**, 739–805 (2009).
[16] J. W. Schmidt and M. R. Moldover, "First-order wetting transition at a liquid–vapor interface," J. Chem. Phys. **79**, 379–387 (1983).
[17] D. Ross, D. Bonn, and J. Meunier, "Observation of short-range critical wetting," Nature **400**, 737–739 (1999).
[18] M. R. Moldover and J. W. Cahn, "An interface phase transition: Complete to partial wetting," Science **207**, 1073–1075 (1980).
[19] D. Bonn, H. Kellay, and G. H. Wegdam, "Experimental observation of hysteresis in a wetting transition," Phys. Rev. Lett. **69**, 1975 (1992).
[20] J. E. Rutledge and P. Taborek, "Prewetting phase diagram of ^{4}He on cesium," Phys. Rev. Lett. **69**, 937 (1992).
[21] H. Zabel, B. Schönfeld, and S. C. Moss, "Critical point wetting in $NbH_{0.31}$," J. Phys. Chem. Solids **42**, 897–900 (1981).
[22] F. Ducastelle, C. Ricolleau, and A. Loiseau, "Order and disorder at interfaces," Mater. Sci. Forum, **155–156**, 367–386 (1994).
[23] K. Ragil, J. Meunier, D. Broseta, J. O. Indekeu, and D. Bonn, "Experimental observation of critical wetting," Phys. Rev. Lett. **77**, 1532 (1996).
[24] N. Shahidzadeh, D. Bonn, K. Ragil, D. Broseta, and J. Meunier, "Sequence of two wetting transitions induced by tuning the Hamaker constant," Phys. Rev. Lett. **80**, 3992 (1998).
[25] R. Pandit, M. Schick, and M. Wortis, "Systematics of multilayer adsorption phenomena on attractive substrates," Phys. Rev. B **26**, 5112–5140 (1982).
[26] J. Mellenthin, A. Karma, and M. Plapp, "Phase-field crystal study of grain-boundary premelting," Phys. Rev. B **78**, 184110 (2008).
[27] M. P. Nightingale and J. O. Indekeu, "Examination of the necessity of complete wetting near critical points in systems with long-range forces," Phys. Rev. B **32**, 3364–3366 (1985).
[28] H. Dosch, L. Mailänder, A. Lied, J. Peisl, F. Grey, R. L. Johnson, and S. Krummacher, "Experimental evidence for an interface delocalization transition in Cu_3Au," Phys. Rev. Lett. **60**, 2382 (1988).
[29] H. Dosch, L. Mailänder, H. Reichert, J. Peisl, and R. L. Johnson, "Long-range order near the $Cu_3Au(001)$ surface by evanescent x-ray scattering," Phys. Rev. B **43**, 13172 (1991).
[30] R. Evans, M. C. Stewart, and N. B. Wilding, "A unified description of hydrophilic and superhydrophobic surfaces in terms of the wetting and drying transitions of liquids," Proc. Natl. Acad. Sci. U. S. A. **116**, 23901–23908 (2019).
[31] A. O. Parry and A. Malijevský, "Surface phase diagrams for wetting with long-ranged forces," Phys. Rev. Lett. **131**, 136201 (2023).
[32] V. Mazauric, A. Finel, and F. Ducastelle, "Theoretical study of antiphase boundaries in fcc alloys: Wetting and layering effects," Phase Transitions **30**, 233–242 (1991).
[33] A. Saúl, B. Legrand, and G. Tréglia, "Link between the surface wetting in Cu(Ag) and the layer-by-layer dissolution mode of a thick Ag deposit on a Cu substrate," Surf. Sci. **331–333**, 805–810 (1995).
[34] P. Wynblatt, A. Saúl, and D. Chatain, "The effects of prewetting and wetting transitions on the surface energy of liquid binary alloys," Acta Mater. **46**, 2337–2347 (1998).
[35] N. Zhou, C. Hu, and J. Luo, "Grain boundary segregation transitions and critical phenomena in binary regular solutions: A systematics of complexion diagrams with universal characters," Acta Mater. **221**, 117375 (2021).

[36]N. Ma, S. A. Dregia, and Y. Wang, "Solute segregation transition and drag force on grain boundaries," Acta Mater. **51**, 3687–3700 (2003).
[37]P. Wynblatt and D. Chatain, "Solid-state wetting transitions at grain boundaries," Mater. Sci. Eng.: A **495**, 119–125 (2008).
[38]J. E. Finn and P. A. Monson, "Prewetting at a fluid-solid interface via Monte Carlo simulation," Phys. Rev. A **39**, 6402–6408 (1989).
[39]W. Schweika, D. P. Landau, and K. Binder, "Surface-induced ordering and disordering in face-centered-cubic alloys: A Monte Carlo study," Phys. Rev. B **53**, 8937–8955 (1996).
[40]K. Binder, F. Haas, and F. Schmid, "Critical phenomena at the surface of systems undergoing a bulk first order transition: Are they understood?," in *Computer Simulation Studies in Condensed-Matter Physics XIV: Proceedings of the Fourteenth Workshop, Athens, GA, USA, February 19–24, 2001* (Springer, 2002), pp. 85–96.
[41]K. Binder, D. Landau, and M. Müller, "Monte Carlo studies of wetting, interface localization and capillary condensation," J. Stat. Phys. **110**, 1411–1514 (2003).
[42]C. A. Becker and Y. Mishin, "Temperature dependence of the pre-wetting transition at the (1 1 1) anti-phase boundary in Ni_3Al: An atomistic study," Modell. Simul. Mater. Sci. Eng. **18**, 074004 (2010).
[43]Y. Li and J. Weissmüller, "Size-dependent phase change in energy storage materials: Comparing the impact of solid-state wetting and of coherency stress," J. Chem. Phys. **162**, 024704 (2025).
[44]P. L. Williams and Y. Mishin, "Thermodynamics of grain boundary premelting in alloys. II. Atomistic simulation," Acta Mater. **57**, 3786–3794 (2009).
[45]K. Binder and D. P. Landau, "Capillary condensation in the lattice gas model: A Monte Carlo study," J. Chem. Phys. **96**, 1444–1454 (1992).
[46]J. Favergeon, J. Y. Huh, W. C. Johnson, and S. M. Wise, "Wetting transitions in a binary thin-film," Metals Mater. Int. **11**, 487–497 (2005).
[47]D. A. Cogswell and M. Z. Bazant, "Theory of coherent nucleation in phase-separating nanoparticles," Nano Lett. **13**, 3036–3041 (2013).
[48]J. Weissmüller, "Coherent phase change in interstitial solutions: A hierarchy of instabilities," Adv. Sci. **11**, 2308554 (2024).
[49]T. Horikawa, D. D. Do, and D. Nicholson, "Capillary condensation of adsorbates in porous materials," Adv. Colloid Interface Sci. **169**, 40–58 (2011).
[50]J. Luo and Y.-M. Chiang, "Wetting and prewetting on ceramic surfaces," Annu. Rev. Mater. Res. **38**, 227–249 (2008).
[51]J. Weissmüller and S. Shi, "Giant compliance and spontaneous buckling of beams containing mobile solute atoms," Acta Mater. **227**, 117696 (2022).
[52]J. M. Sanchez and D. de Fontaine, "The fcc Ising model in the cluster variation approximation," Phys. Rev. B **17**, 2926–2936 (1978).
[53]K. Binder and D. P. Landau, "Wetting and layering in the nearest-neighbor simple-cubic Ising lattice: A Monte Carlo investigation," Phys. Rev. B **37**, 1745 (1988).
[54]K. Binder and D. P. Landau, "Critical phenomena at surfaces," Physica A **163**, 17–30 (1990).
[55]The original result, Eq. (3.8) in Ref. 1, is derived by counting bonds originating at "A" type atoms only, for an A-B solution. Our Eq. (11) corrects that scheme by accounting also for the energy contributed by "B" atoms at the origin. The combination of our Eqs. (9) and (11) is invariant under $\{x \to 1 - x, \nabla^2 x \to -\nabla^2 x\}$, as is required for the bond-counting model. The results for the gradient-square representation, and specifically for κ, are not affected.
[56]Y. Mishin, "Solute drag and dynamic phase transformations in moving grain boundaries," Acta Mater. **179**, 383–395 (2019).
[57]A similar approach is reported in the layer-model study of grain boundary wetting, Ref. 37.
[58]S. J. Dillon, M. Tang, W. C. Carter, and M. P. Harmer, "Complexion: A new concept for kinetic engineering in materials science," Acta Mater. **55**, 6208–6218 (2007).
[59]W. D. Kaplan, D. Chatain, P. Wynblatt, and W. C. Carter, "A review of wetting versus adsorption, complexions, and related phenomena: *The rosetta stone of wetting*," J. Mater. Sci. **48**, 5681–5717 (2013).
[60]J. W. Cahn, "Wetting and non-wetting near critical points in solids," Physica A **279**, 195–202 (2000).
[61]M. E. Gurtin, J. Weissmüller, and F. Larché, "A general theory of curved deformable interfaces in solids at equilibrium," Philos. Mag. A **78**, 1093–1109 (1998).
[62]L. Bourchtein and A. Bourchtein, *Theory of Infinite Sequences and Series* (Birkhäuser, Cham, 2021).